Progress In Electromagnetics Research C, Vol. 30, 253–265, 2012

HIGH-ORDER DUAL-BAND BANDPASS FILTER WITH INDEPENDENTLY CONTROLLABLE FREQUENCIES AND BANDWIDTHS

Q.-X. Chu and Z.-H. Li*

School of Electronic and Information Engineering, South China University of Technology, Guangzhou, Guangdong 510640, China

Abstract—A multi-stub-loaded resonator is presented in this paper. The resonators can be conveniently applied to design high-order dual-band bandpass filters (BPFs). Base on the analysis of the resonator, the first two even-mode resonant frequencies are controlled independently by the lengths of the loaded stubs. Two high-order dual-band BPFs using the first two even-mode resonant frequencies of the multi-stub-loaded resonators are proposed. The bandwidth of each passband can be adjusted independently by the coupling strength of the adjacent resonators. This paper deals with the analysis and design of the proposed high-order dual-band BPFs as well as the experimental validations of the predicted dual-band performance.

1. INTRODUCTION

Emerging wireless standards produce new consumer systems, such as wireless local area networks (WLANs), global system for mobile communications (GSM), and worldwide interoperability for microwave access (WiMAX). With the ever-increasing demand for these applications in the communication market all around the world, dual- or multi-band filters have enabled a single wireless system to support dual- or multi-band operations in [1]. To meet the needs, much research regarding them has been carried out and various design approaches have been proposed. For instance, stepped impedance resonators (SIRs) had been implemented to realize dual-band BPFs. The dual-band BPFs using SIRs had attractive features such as, simple and compact structure in [2, 3], low insertion loss in [4], high isolation

Received 25 May 2012, Accepted 2 July 2012, Scheduled 5 July 2012

* Corresponding author: Zhi-Hui Li (li.zhihui@mail.scut.edu.cn).

in [5]. However, independently controllable bandwidths and passband frequencies were not mentioned in these papers. Another method was to realize dual-band BPFs by using stub-loaded resonators in [6–8]. Theoretical analysis showed that the even-mode resonant frequencies of stub-loaded resonators could be conveniently tuned without affecting the odd-mode resonant frequencies. All of the aforementioned filters were only considered the second-order dual-band BPFs. For high selectivity, some researchers were interested in high-order dual-band BPFs. The SIRs were applied to high-order dual-band BPFs with a good analytical method in [9]. Stub-loaded resonators were proposed to design compact high-order dual-band BPFs in [10]. However, both centre frequencies and bandwidths of these high-order filters were dependent.

In this paper, two high-order dual-band BPFs using multi-stub-loaded resonators are presented. Based on our investigation, the multi-stub-loaded resonators are appropriate to build up high-order dual-band BPFs. Moreover, the first two even-mode resonant frequencies can be conveniently tuned by the lengths of the open loaded stubs. The coupling strength of each passband is independently determined by the coupling spacing between the resonators. When the external quality factors remain unchanged, the bandwidths of the two passbands can be controlled independently by the coupling spacing without affecting each other. Thus the proposed high-order dual-band BPFs have attractive features of independently controllable bandwidths and centre passband frequencies. To validate the concept, two microstrip dual-band BPFs centered at 3.5 GHz (WiMAX)/5.2 GHz (WLANs) with different bandwidth ratios. One is a fourth-order dual-band filter. The other is a fifth-order dual-band filter. These two filters are designed, fabricated, and measured.

2. CHARACTERISTICS OF THE MULTI-STUB-LOADED RESONATOR

Figure 1(a) is basic structure of the proposed resonator. It is a conventional transmission line in the vertical position with two sets of open loaded stubs. As the resonator is symmetrical, the odd-even mode method can be applied to analyse the resonant characteristics. The resonator is decomposed into odd-mode model and even-mode model indicated in Figures 1(b) and (c). The even-mode model consists of a transmission line with impedance Z_3, electrical length θ_3, and physical length l_3 in the vertical position, and two open loaded stubs in the horizontal position. One open loaded stub is with impedance Z_1, electrical length θ_1, and physical length l_1. The other open loaded

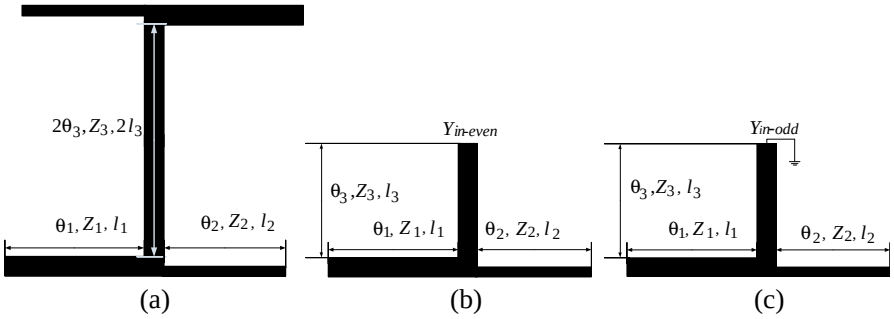

Figure 1. (a) The multi-stub-loaded resonator. (b) The even-mode model. (c) The odd-mode model.

stub is with impedance Z_2, electrical length θ_2, and physical length l_2. The basic parameters of the odd-mode model are the same as the even-mode model, but the end of the transmission line of the odd-mode model is grounded. In this paper, the characteristic impedances are selected to be different, implying $Z_1 \neq Z_2 \neq Z_3$

The even-mode model or odd-mode model is equivalent to three transmission lines in parallel, thus the even-mode resonant condition can be obtained as follows:

$$K_1 \tan\theta_1 + K_2 \tan\theta_2 + \tan\theta_3 = 0 \tag{1}$$

the odd-mode resonant condition can be expressed as follows:

$$K_1 \tan\theta_1 + K_2 \tan\theta_2 - \cot\theta_3 = 0 \tag{2}$$

where $K_1 = Z_3/Z_1$ and $K_2 = Z_3/Z_2$ are defined as impedance ratios.

For further discussing the characteristics of the resonator, one resonator is built on a substrate with dielectric constant $\varepsilon_r = 2.55$, loss tangent $\delta = 0.0029$, and thickness $h = 0.8\,\text{mm}$. Full-wave simulation is carried out by using software IE3D. The resonant frequencies of the resonator can be obtained by the simulated result shown in Figure 2. The first, the third, the second, and the fourth resonant frequencies are named as f_{odd1}, f_{odd2}, f_{even1}, and f_{even2}, respectively. When only the physical length L_1 is tuned, only f_{even2} is unchanged. In the same way, when only the physical length L_2 is changed, f_{odd1} and f_{even1} are fixed. Thus the even-mode resonant frequencies can be independently controlled by the lengths of the loaded stubs. In this paper, only the even-mode resonant frequencies are used and the odd-mode resonant frequencies are restrained.

In order to simplify the analysis of the resonant characteristics, only even-mode resonant frequencies are taken into account. A chart,

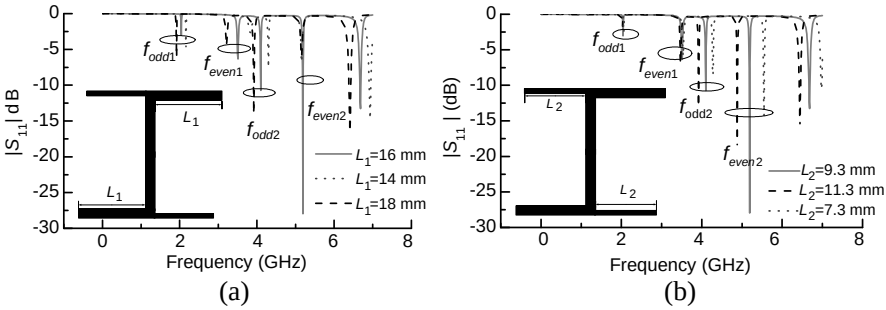

Figure 2. (a) Shows the relationship between the resonant frequencies and the physical length L_1, while the physical length L_2 is unchanged. (b) Displays the relationship between the resonant frequencies and the physical length L_2, when the physical length L_1 is fixed.

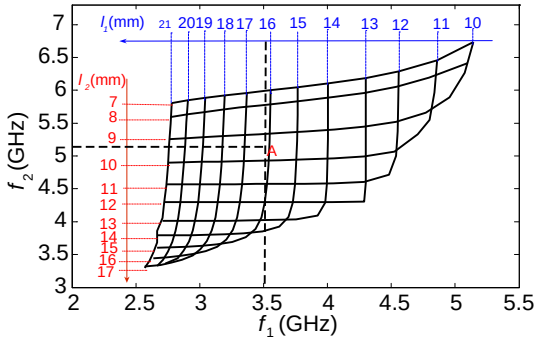

Figure 3. Frequencies f_1 and f_2 versus the physical lengths l_1 and l_2, considering that $l_3 = 11\,\text{mm}$, $K_1 = 0.6$, and $K_2 = 0.4$. The resonator is built on a substrate with dielectric constant $\varepsilon_r = 2.55$, loss tangent $\delta = 0.0029$, and thickness $h = 0.8\,\text{mm}$.

which is shown in Figure 3, reveals that the relationship between the first two even-mode frequencies (f_1, f_2) and the physical lengths (l_1, l_2). It is extracted by Formula (3). It is found that f_1 is determined by the physical length l_1 and the physical length l_2 only affects f_2. Frequencies f_1 and f_2 can be controlled independently without affecting each other.

$$K_1 \tan(\alpha \cdot f \cdot l_1) + K_2 \tan(\alpha \cdot f \cdot l_2) + \tan(\alpha \cdot f \cdot l_3) = 0 \qquad (3)$$

where α is $2\pi\sqrt{\varepsilon_r}/c$, c is the speed of light in vacuum, ε_r is dielectric constant.

3. DESIGN PROCESS OF HIGH-ORDER DUAL-BAND FILTER

3.1. Filter Configuration

A fourth-order dual-band BPF using multi-stub-loaded resonators is presented in Figure 4. It consists of four resonators, namely, resonator I, resonator II, resonator III, and resonator IV. Resonator I and II are exactly the same, and resonator III and resonator IV are also identical. The dimension of two resonators which are connected with each other to be a resonator III is exactly the same as the ones of resonator I. Resonator I is equivalent to the even-mode model of resonator III. Only even-mode signals can pass resonator I or resonator II. That is to say, the odd-mode resonant frequencies can not be energized in resonator III and IV.

The fourth-order dual-band filter is designed at frequencies $f_1 = 3.5\,\text{GHz}$ and $f_2 = 5.2\,\text{GHz}$, which is built on a substrate with dielectric constant $\varepsilon_r = 2.55$, loss tangent $\delta = 0.0029$, and thickness $h = 0.8\,\text{mm}$. For the fourth-order filter, a Chebyshev lowpass prototype with a passband ripple of 0.1 dB is chosen, the element values are $g_0 = 1$, $g_1 = 1.1088$, $g_2 = 1.3061$, $g_3 = 1.7703$, $g_4 = 08180$, and $g_5 = 1.3554$. Under the conditions of $K_1 = 0.6$ and $K_2 = 0.4$, impedance Z_3 is selected to be $50\,\Omega$ (line width $W_3 = 2.2\,\text{mm}$), so impedance Z_1 is $83.3\,\Omega$ (line width $W_1 = 1\,\text{mm}$) and Z_2 is $125\,\Omega$ (line width $W_2 = 0.4\,\text{mm}$), respectively. According to frequencies f_1 and f_2 marked as crossing point 'A' in Figure 3, the parameters of the resonator can be obtained as follow: $l_2 = L_2 + L_5 = 9.2\,\text{mm}$, $l_1 = L_1 + L_4 = 16.2\,\text{mm}$, and $l_3 = L_3 = 11\,\text{mm}$.

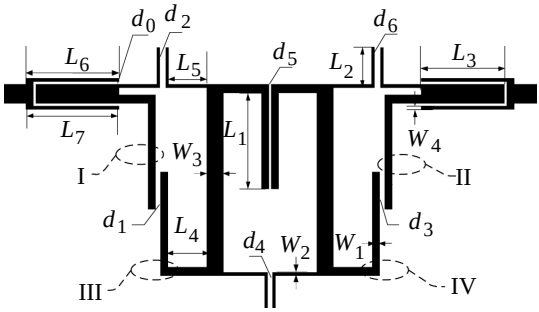

Figure 4. Layout of the fourth-order dual-band BPF.

3.2. Feed Circuit and Resonator Coupling

The coupling scheme in [11] is used as the input/output of the proposed filter because it has more degrees of freedom in the design process. Four parameters, including d_0, L_6, L_7, and W_4 shown in Figure 4, can be tuned to obtain different external quality factors. Here, the external quality factors Q_{ek} are extracted by [12]

$$Q_{ek} = f_k/\delta f_{\pm 90^0}, \quad k = 1 \text{ or } 2 \tag{4}$$

where f_k and $f^{\circ}_{\pm 90}$ represent the resonant frequencies and the absolute bandwidth between the $\pm 90^{\circ}$ points of the S_{11} phase response for the coupling structure related to each band.

Given the desired Q_{e1} and Q_{e2}, the parameters of the coupled-line structure can be determined by the curves shown in Figure 5. The coupled-line length and the coupling spacing can be selected properly to meet different bandwidths. It is found that independent controllability is very limited in Q_{e1} or Q_{e2} and also the tuning ranges of Q_{e1} and Q_{e2} are limited. More design data can be obtained by choosing different combinations of L_6, L_7, W_4, and d_0, while it is needed.

The coupling coefficients between the adjacent resonators are determined by [12]

$$(M_{i,i+1})_k = \frac{\Delta_k}{\sqrt{g_i g_{i+1}}}, \quad \text{for } i = 1 \text{ to } N-1, \text{and } k = 1 \text{or } 2 \tag{5}$$

where Δ_k (i.e., $k = 1$ or $k = 2$) is defined as the fractional bandwidth of the first or second passband. $(M_{i,i+1})_1$ and $(M_{i,i+1})_2$ denote the coupling coefficients of the first and second passbands, respectively. The parameter N is the order of the filter.

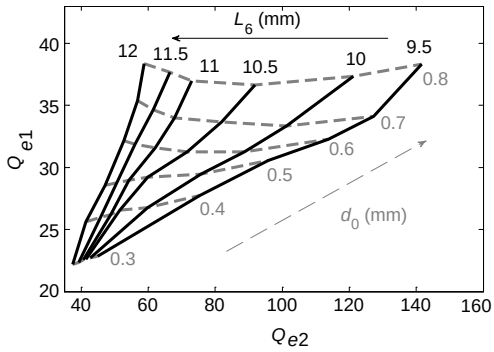

Figure 5. Simulated Q_{e1} and Q_{e2} under different coupled-line length L_6 and coupling spacing d_0 with $L_6 = L_7$ and $W_4 = 0.3\,\text{mm}$.

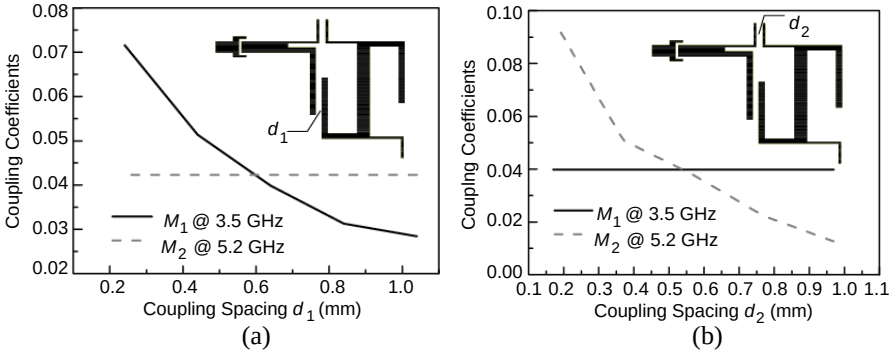

Figure 6. Simulated the coupling coefficients under different coupling spacing. (a) d_1, while $d_2 = 0.67$ mm is fixed. (b) d_2, when $d_1 = 0.53$ mm is fixed.

The coupling coefficients $M_{i,i+1}$ between the adjacent resonators can be extracted by [12]

$$M_{i,i+1} = \pm\frac{1}{2}\left(\frac{f_2}{f_1} + \frac{f_1}{f_2}\right)\sqrt{\left(\frac{f_{p2}^2 - f_{p1}^2}{f_{p2}^2 + f_{p1}^2}\right)^2 - \left(\frac{f_2^2 - f_1^2}{f_1^2 + f_2^2}\right)^2} \quad (6)$$

where f_1 and f_2 are two resonant frequencies at the two resonators and f_{p1} and f_{p2} defined to be the lower and higher resonant modes of coupled resonators at resonant frequency f_1 or f_2.

The relationship between the coupling coefficients and the coupling spacing (d_1, d_2) is shown in Figure 6. It can be seen that the couplings of these even-mode resonances (between the inner resonators) are independently controlled by the coupling spacing d_1 or d_2.

According to the aforementioned discussion, the overall design steps of this kind of high-order dual-band filters are summarized as follows:

Step 1: Confirm the dual-band filter specifications, including the centre frequencies (f_1, f_2), the fractional bandwidths (Δ_1, Δ_2), the order (N) of the filter, and the low-pass prototype elements g_i, $i = 0, 1, \ldots, N, N+1$.

Step 2: The structural parameters of the multi-stub-loaded resonator can be achieved by the curves in Figure 3, including l_1, l_2, l_3, K_1, and K_2.

Step 3: Basing on Δ_1, Δ_2, N, and g_i, we can calculate the parameters, including the external quality factors Q_{e1} and Q_{e2}, and the coupling coefficients M_1 and M_2. Depending on Q_{e1} and Q_{e2}, the parameters including, L_6, L_7, W_4, and d_0 of the coupling structure, are

gotten from the gridlines in Figure 5. In the same way, the coupling spacing can be obtained by Figure 6.

Step 4: Combine the parameters from *Step 2* and *Step 3* above, the filter with initial parameters is simulated by a full-wave EM simulator. The final parameters of the filter are determined after optimizing through the EM simulator.

4. DESIGN EXAMPLES

4.1. One Fourth-order Dual-band Filter with $\Delta_1/\Delta_2 = 1$

According to the dual-band filter specifications aforementioned, the physical parameters of the resonator have been obtained in Section 3.

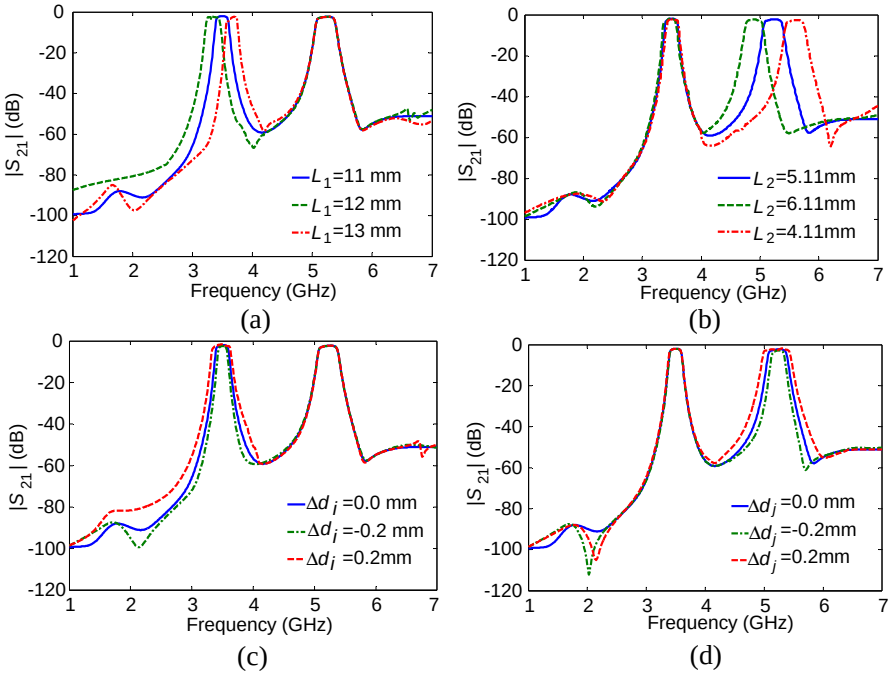

Figure 7. (a) Frequencies versus the length L_1, while the length $L_2 = 5.11\,\text{mm}$ is fixed. (b) Frequencies versus the length L_2, when the length $L_1 = 11\,\text{mm}$ is fixed. (c) The lower bandwidth versus different coupling spacing variation Δd_i, while the coupling spacing d_2, d_4, and d_6 remain unchanged. (d) The higher bandwidth versus different coupling spacing variation Δd_j, when the coupling spacingd_1, d_3, and d_5 are fixed.

The fractional bandwidths of the two passbands are defined as follows: $\Delta_1 = \Delta_2 = 4\%$. The external quality factors can be deduced as follows: $Q_{e1} = Q_{e2} = 27.7$; According to Q_{e1} and Q_{e2}, the parameters of the feed structure are properly obtained by Figure 5 as follows: $L_6 = L_7 = 11\,\text{mm}$, $W_4 = 0.4\,\text{mm}$, and $d_0 = 0.3\,\text{mm}$. The coupling coefficients can be calculated by the element values of Chebyshev lowpass prototype: $(M_{12})_1 = 0.0332$, $(M_{23})_1 = 0.0263$, $(M_{34})_1 = 0.0276$, $(M_{12})_2 = 0.0332$, $(M_{23})_2 = 0.0263$, $(M_{34})_2 = 0.0276$, where $(M_{12})_1$, $(M_{23})_1$, and $(M_{34})_1$ indicate the coupling coefficients of the first passband between the adjacent resonators, and $(M_{12})_2$, $(M_{23})_2$, and $(M_{34})_2$ denote the coupling coefficients of the second passband. According to the above mentioned coupling coefficients, the coupling spacing between the adjacent resonators at f_1 can be obtained by Figure 6(a) as follows: $d_1 = 0.82\,\text{mm}$, $d_3 = 0.92\,\text{mm}$, and $d_5 = 0.9\,\text{mm}$. In the same way, the coupling spacing of the second passband can be obtained by Figure 6(b) as follows: $d_2 = 0.67\,\text{mm}$, $d_4 = 0.8\,\text{mm}$, and $d_6 = 0.75\,\text{mm}$.

As can be seen in Figure 7, when the length L_1 is tuned (all the other parameters are fixed), only frequency f_1 (3.5 GHz) is changed. Likewise, tune the length L_2, only frequency f_2 (5.2 GHz) is affected. Remain the input/output structure unchanged, when only the coupling spacing d_1, d_3, and d_5 are changed, the lower bandwidth can be adjusted, whereas the higher bandwidth remain unaltered. Similarly, the higher bandwidth is affected independently by the coupling spacing

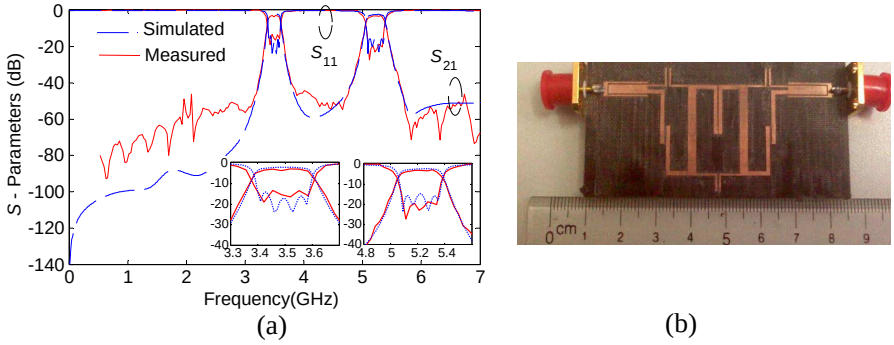

Figure 8. Simulated (dashed lines) and measured (solid lines) results of the dual-band filter. (a) Scattering parameters. (b) Photograph of the fourth-order dual-band filter. ($d_0 = 0.3$, $d_1 = 0.53$, $d_2 = 0.67$, $d_3 = 0.63$, $d_4 = 0.45$, $d_5 = 0.65$, $d_6 = 0.72$, $L_1 = 11$, $L_2 = 4.23$, $L_3 = 11$, $L_4 = 5.11$, $L_5 = 5.02$, $L_6 = 11.3$, $L_7 = 11.3$, $W_1 = 1.0$, $W_2 = 0.4$, $W_3 = 2.2$, $W_4 = 0.4$. All are in mm.).

d_2, d_4, and d_6. Here Δd_i is defined as variation of the coupling spacing d_1, d_3, and d_5, which are changed at the same time. In the same way, Δd_j denotes that the coupling spacing d_2, d_4, and d_6 are changed at the same time.

The simulated and measured results of the fabricated filter are shown in Figure 8. The size of the filter is approximately $0.8\lambda_0 \times 0.35\lambda_0$, where λ_0 is the full wavelength of frequency at $f_1 = 3.5$ GHz. It can be seen that the measured and simulated results are in good agreement. The lower passband of 3.5 GHz has 2.2 dB insertion loss and better than 15 dB return loss. The higher passband of 5.2 GHz has 2.2 dB insertion loss and better than 15 dB return loss. The rejection level between the two passbands is better than 50 dB from 3.88 to 4.62 GHz. The 3 dB fractional bandwidths (FBWs) are $\Delta_1 = 4.2\%$ and $\Delta_2 = 4.1\%$, respectively.

4.2. One Fifth-order Dual-band Filter with $\Delta_1/\Delta_2 > 1$

The second example is a fifth-order dual-band filter shown in Figure 9 with the centre frequencies located at $f_1 = 3.5$ GHz and $f_2 = 5.2$ GHz. The fractional bandwidths of the two passbands are $\Delta_1 = 4.5\%$ and $\Delta_2 = 3.5\%$, respectively. For the fifth-order filter, a Chebyshev lowpass prototype with a passband ripple of 0.1 dB is chosen, the elements values are $g_0 = 1$, $g_1 = 1.1468$, $g_2 = 1.3712$, $g_3 = 1.9750$, $g_4 = 1.3712$, $g_5 = 1.1468$, and $g_6 = 1$. The physical parameters of the resonator have been obtained in Section 3. The external quality factors can be deduced as follows: $Q_{e1} = 25.5$, $Q_{e2} = 32.8$. According to Q_{e1} and Q_{e2}, the proper input/output coupled-line parameters are obtained by Figure 5 as follows: $L_{16} = L_{17} = 11.5$ mm, $W_{14} = 0.4$ mm, and $d_{10} = 0.43$ mm. The coupling coefficients can be calculated by the element values of the chebyshev lowpass prototype: $(M_{12})_{11} = 0.0357$,

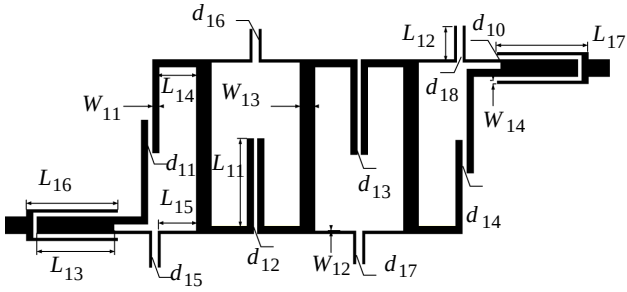

Figure 9. Layout of the fifth-order dual-band BPF.

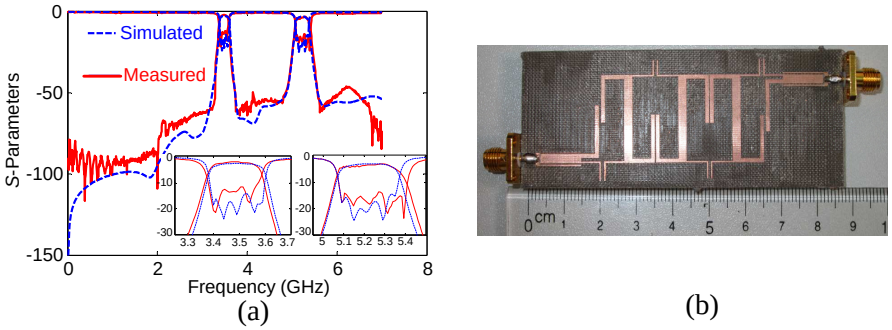

Figure 10. Simulated (dashed lines) and measured (solid lines) results of the dual-band filter. (a) Scattering parameters. (b) Photograph of the fifth-order dual-band filter. ($d_{10} = 0.43$, $d_{11} = 0.6$, $d_{12} = 0.4$, $d_{13} = 0.4$, $d_{14} = 0.6$, $d_{15} = 0.8$, $d_{16} = 0.7$, $d_{17} = 0.7$, $d_{18} = 0.8$, $L_{11} = 11$, $L_{12} = 4.23$, $L_{13} = 11$, $L_{14} = 5.21$, $L_{15} = 5.4$, $L_{16} = L_{17} = 11.5$, $W_{11} = 1.0$, $W_{12} = 0.4$, $W_{13} = 2.2$, $W_{14} = 0.4$. All are in mm.).

$(M_{23})_{11} = 0.0273$, $(M_{34})_{11} = 0.0273$, $(M_{45})_{11} = 0.0357$, $(M_{12})_{22} = 0.0279$, $(M_{23})_{22} = 0.0213$, $(M_{34})_{22} = 0.0213$, and $(M_{45})_{22} = 0.0279$, where $(M_{12})_{11}$, $(M_{23})_{11}$, $(M_{34})_{11}$ and $(M_{45})_{11}$ indicate the coupling coefficients of the lower passband, and $(M_{12})_{22}$, $(M_{23})_{22}$, $(M_{34})_{22}$, and $(M_{45})_{22}$ denote the coupling coefficients of the higher passband. The coupling spacing between the adjacent resonators can be achieved by Figure 6 as follows: $d_{11} = 0.65$ mm, $d_{12} = 0.84$ mm, $d_{13} = 0.84$ mm, $d_{14} = 0.65$ mm,$d_{15} = 0.72$ mm, $d_{16} = 0.82$ mm, $d_{17} = 0.82$ mm, and $d_{18} = 0.72$ mm.

In this design, the fifth-order filter has the similar features like the aforementioned fourth-order filter in part A of this section, including controllable frequencies and tunable bandwidths independently. The simulated and measured results of the fabricated filter are depicted in Figure 10. It is seen that the measured and simulated results are in good agreement. The lower passband of 3.5 GHz has 2.5 dB insertion loss and better than 12 dB return loss. The higher passband of 5.2 GHz has 2.8 dB insertion loss and better than 14 dB return loss. The rejection level between the two passbands is better than 50 dB from 3.72 to 4.82 GHz. The 3 dB fractional bandwidths (FBWs) are $\Delta_1 = 4.9\%$ and $\Delta_2 = 4\%$.

5. CONCLUSION

This paper has presented two high-order dual-band BPFs using multi-stub-loaded resonators and also given exhaustive design steps to design the high-order dual-band BPFs. Measured results are found to be in good agreement with simulated ones. They reveal that the presented filters achieve high isolation and good selectivity at passband edges. As can be seen in Figure 3, when the length l_1 is tuned, only f_1 is changed and f_2 keeps fixed. In the same way, the length l_2 mainly controls f_2 without affecting f_1. The couplings of these even-mode resonances (between the inner resonators) are independently controlled by the coupling spacing shown in Figure 6. Simulated results also show that passband frequencies and bandwidths of the proposed filters are flexibly independently controlled. The tunable features indicate that the proposed filters have a potential to be utilized in wireless communication systems with different frequencies and bandwidths.

ACKNOWLEDGMENT

This work was supported by the National Natural Science Foundation of China (61171029 and 61101016).

REFERENCES

1. Chang, S. F. R., W. L. Chen, S. C. Chang, C. K. Tu, C. L. Wei, C. H. Chien, C. H. Tsai, J. Chen, and A. Chen, "A dual-band RF transceiver for multi-standard WLAN applications," *IEEE Trans. Microw. Theory Tech.*, Vol. 53, No. 3, 1048–1055, Mar. 2005.
2. Weng, M.-H., C.-H. Kao, and Y.-C. Chang, "A compact dual-band bandpass filter using cross-coupled asymmetric SIRs for WLANs," *Journal of Electromagnetic Waves and Application*, Vol. 24, Nos. 2–3, 161–168, 2010.
3. Ma, D.-C., Z.-Y. Xiao, L.-L. Xiang, X.-H. Wu, C.-Y. Huang, and X. Kou, "Compact dual-band bandpass filter using folded SIR with two stubs for WLAN," *Progress In Electromagnetic Research*, Vol. 117, 357–364, 2011.
4. Weng, M. H., H. W. Wu, and Y. K. Su, "Compact and low loss dual-band bandpass filter using pseudo-interdigital stepped impedance resonators for WLANs," *IEEE Microw. Wireless Compon. Lett.,* Vol. 17, No. 3, 187–189, Mar. 2007.
5. Wu, Y.-L., C. Liao, and X.-Z. Xiong, "A dual-wideband bandpass filter based on E-shaped microstrip SIR with improved upper-

stopband performance," *Progress In Electromagnetics Research*, Vol. 108, 141–153, 2010.

6. Zhang, X. Y., J. X. Chen, and Q. Xue, "Dual-band bandpass filter using stub-loaded resonators," *IEEE Microw. Wireless Compon. Lett.*, Vol. 17, No. 8, 583–585, Aug. 2007.
7. Deng, H.-W., Y.-J. Zhao, X.-S. Zhang, L. Zhang, and W. Zhao, "Compact dual-mode open stub-loaded resonator and BPF," *Progress In Electromagnetics Research Letters*, Vol. 14, 119–125, 2010.
8. Chen, F. C., Q. X. Chu, and Z. H. Tu, "Design of compact dual-band bandpass filter using short stub loaded resonator," *Microw. Opt. Technol. Lett.,* Vol. 51, No. 4, 959–963, Apr. 2009.
9. Chang, W. S. and C. Y. Chang, "Analytical design of microstrip short-circuit terminated stepped-impedance resonator dual-band filters," *IEEE Trans. Microw. Theory Tech.*, Vol. 59, No. 7, 1730–1739, Jul. 2011.
10. Mondal, P. and M. K. Mandal, "Design of dual-band bandpass filters using stub-loaded open-loop resonators," *IEEE Trans. Microw. Theory Tech.,* Vol. 56, No. 1, 150–155, Jan. 2008.
11. Zhang, Y. P. and M. Sun, "Dual-band microstrip bandpass filter using stepped-impedance resonators with new coupling schemes," *IEEE Trans. Microw. Theory Tech.*, Vol. 54, No. 10, 3779–3785, Oct. 2006.
12. Hong, J. S. and M. J. Lancaster, *Microstrip Filter for RF/Microwave Applications,* Wiley, New York, 2001.